Solution Structure of a Conserved Domain of Antizyme: A Protein Regulator of Polyamines[†,‡]

David W. Hoffman,* Donald Carroll, Nadia Martinez, and Marvin L. Hackert*

Department of Chemistry and Biochemistry, Institute for Cellular and Molecular Biology, University of Texas, Austin, Texas 78712

Received June 6, 2005; Revised Manuscript Received July 1, 2005

ABSTRACT: Antizyme and its isoforms are members of an unusual yet broadly conserved family of proteins, with roles in regulating polyamine levels within cells. Antizyme has the ability to bind and inhibit the enzyme ornithine decarboxylase (ODC), targeting it for degradation at the proteasome; antizyme is also known to affect the transport of polyamines and interact with the antizyme inhibitor protein (AZI), as well as the cell-cycle protein cyclin D1. In the present work, NMR methods were used to determine the solution structure of a stable, folded domain of mammalian antizyme isoform-1 (AZ-1), consisting of amino acid residues 87−227. The protein was found to contain eight β strands and two α helices, with the strands forming a mixed parallel and antiparallel β sheet. At the level of primary sequence, antizyme is not similar to any protein of known structure, and results show that antizyme exhibits a novel arrangement of its strands and helices. Interestingly, however, the fold of antizyme is similar to that found in a family of acetyl transferases, as well as translation initiation factor IF3, despite a lack of functional relatedness between these proteins. Structural results, combined with amino acid sequence comparisons, were used to identify conserved features among the various homologues of antizyme and their isoforms. Conserved surface residues, including a cluster of acidic amino acids, were found to be located on a single face of antizyme, suggesting this surface is a possible site of interaction with target proteins such as ODC. This structural model provides an essential framework for an improved future understanding of how the different parts of antizyme play their roles in polyamine regulation.

Antizyme was first identified as a polyamine-inducible inhibitor of the enzyme ornithine decarboxylase (ODC)[1] in rat liver (*1*). ODC is the first and rate-limiting enzyme in the pathway of polyamine biosynthesis, converting ornithine to putrescine, which is a precursor of the polyamines spermidine and spermine. Polyamines bind to RNA and chromosomal DNA and have roles in the compaction of DNA, cell cycle, apoptosis, gene expression, embryonic development, and neurochemistry and are essential for normal cell growth and proliferation (reviewed in refs *2* and *3*). Antizyme is a key component in the mechanism for the regulation of cellular polyamine levels (*4*, *5*).

Antizyme is an unusual protein in several respects. It is known to catalyze the ATP-dependent but ubiquitin-independent degradation of ODC by the 26S proteasome (*6*−*10*). This process is remarkable because of its rarity. Normally, degradation at the proteasome requires the attachment of polyubiquitin chains to the target protein. For many years, ODC was the only well-characterized, genuine substrate for ubiquitin-independent degradation by the proteasome. Recently, however, the cyclin-dependent kinase inhibitor p21 has also been shown to undergo regulated degradation without ubiquitination (*11*). Antizyme is also unusual in the way that it is translated at the ribosome. Matsufuji and co-workers (*12*) and also Rom and Kahana (*13*) have shown *in vitro* that polyamines are able to stimulate a programmed +1 frameshift during translation of the antizyme messenger RNA, providing a means for regulating the protein. This was the first example of a mammalian cellular gene expressed by programmed frameshifting, an exceedingly rare event only occasionally observed even for bacterial and viral genes. The +1 frameshift site occurs within the coding region for antizyme, and the frameshift-stimulating ability is conserved from yeast to mammals (*14*). A pseudoknot structure within the antizyme messenger RNA and high concentrations of polyamines seem to be critical for stimulating the frameshifting events (*12*, *13*, *15*−*17*).

At least three isoforms of antizyme are present in humans (*16*, *18*) and each appears to have a specific role in regulating polyamine metabolism. Isoform-1 of antizyme (AZ-1) is ubiquitously expressed in the body and is capable of binding and promoting the degradation of ODC. AZ-1 also has the

[†] This work was supported by Grants F-1353 (to D.W.H.) and F-1219 (to M.L.H.) from the Welch Foundation.

[‡] PDB identification number: 1ZO0.

* To whom correspondence should be addressed: Department of Chemistry and Biochemistry, Institute for Cellular and Molecular Biology, University of Texas, Austin, TX, 78712. E-mail: m.hackert@mail.utexas.edu. Telephone: 512-471-1105. Fax: 512-471-8696 (M.L.H.); Department of Chemistry and Biochemistry, Institute for Cellular and Molecular Biology, University of Texas, Austin, TX, 78712. E-mail: dhoffman@mail.utexas.edu. Telephone: 512-471-7859. Fax: 512-471-8696 (D.W.H.).

[1] Abbreviations: AZ-1, antizyme isoform-1; AZ-2, antizyme isoform-2; AZ-3, antizyme isoform-3; AZBE, antizyme-binding element; AZI, antizyme inhibitor protein; DSS, 2,2-dimethyl-2-silapentane-5-sulfonate; IPTG, isopropyl-β-D-thiogalactopyranoside; NMR, nuclear magnetic resonance; NOE, nuclear Overhauser effect; ODC, ornithine decarboxylase.

10.1021/bi051081k CCC: $30.25
Published on Web 08/10/2005

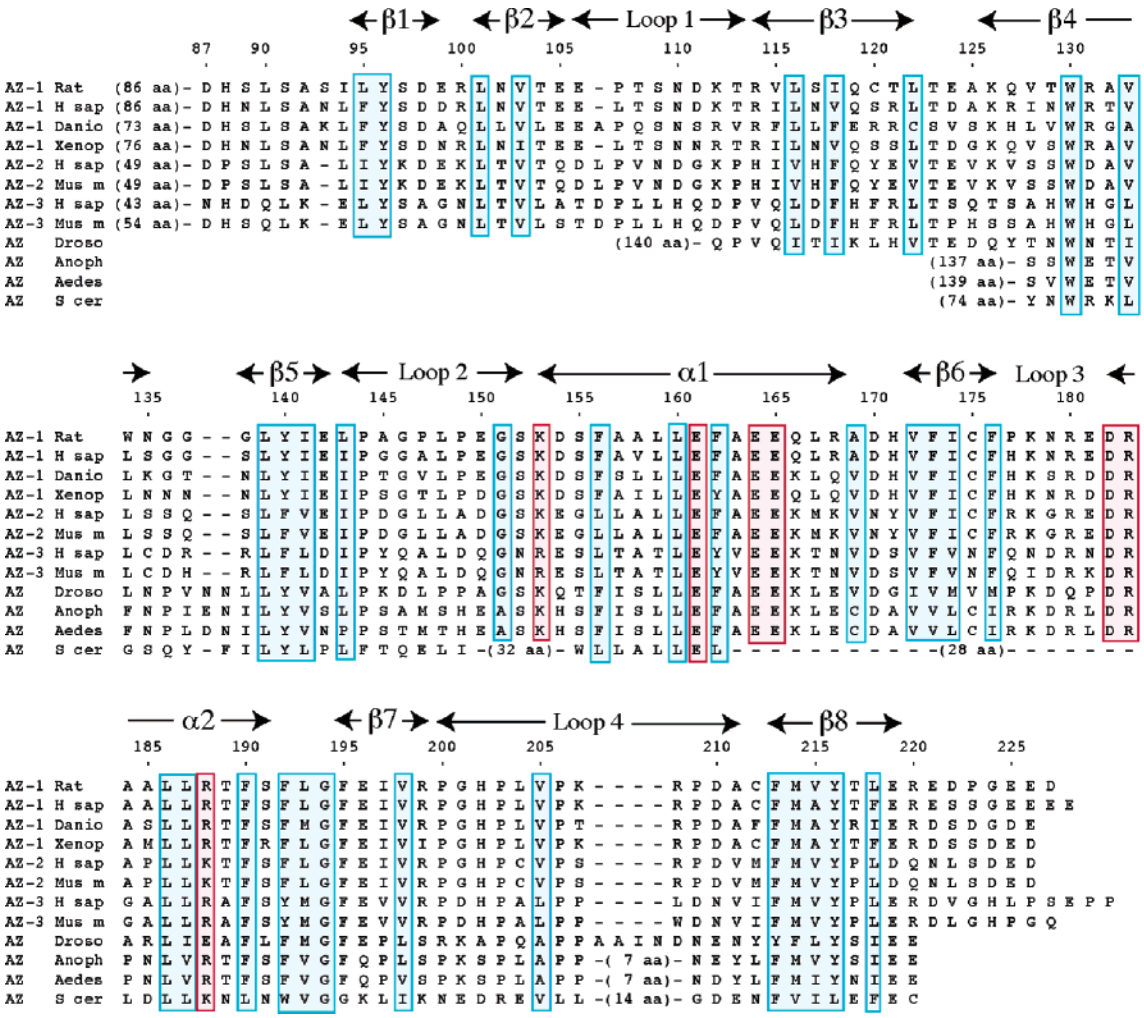

FIGURE 1: Alignment of the amino acid sequences of antizyme proteins from a diverse set of eukarya. Sequences are shown for antizyme isoform-1 from *Rattus norvegicus* (AZ-1 Rat), *Homo sapiens* (AZ-1 H sap), *Danio rerio* (AZ-1 Danio), and *Xenopus laevis* (AZ-1 Xenop). Isoform-2 and isoform-3 sequences from *Homo sapiens* and *Mus musculus* are also aligned, as are homologues from *Drosophila melanogaster* (Droso), *Anopheles gambiae* (Anoph), and *Aedes aegypti* (Aedes) that are similar to the vertebrate anitizymes. The part of the antizyme sequence from *Saccharomyces cerevisiae* (S cer) that displays an identifiable sequence similarity to the antiyzmes from the multicellular organisms is also included in the alignment (*53*). The residues in the N-terminal region of each protein that do not exhibit clear similarity to those of the mammalian antizyme are not included in the alignment. Most of the conserved amino acids of anitzyme are concentrated toward the C terminus of each protein. Well-conserved (and mostly hydrophobic) residues that are judged to be important for structural purposes are boxed in blue. Conserved hydrophilic residues that are accessible on the protein surface are boxed in red; these are the most likely candidates for mediating intermolecular interactions, such as with ODC. Although only 12 sequences are shown in the figure, a larger set of sequences was compared in deciding which residues are relatively well-conserved.

ability to repress polyamine levels by inhibiting the transporter for the uptake of extracellular polyamines (*19*). AZ-1 from rats (the subject of the present study) is 90% identical to human AZ-1 (Figure 1); these proteins contain 227 and 228 amino acids, respectively. Isoform-2 of antizyme (AZ-2) does not appear to stimulate ODC degradation at the proteasome but does maintain the ability to negatively regulate polyamine transport (*20*). Mutating just two residues of rat AZ-1 (Arg131 and Ala145) to Asp as found in AZ-2 can change the properties of AZ-1 to those similar to AZ-2 (*21*). A third isoform, AZ-3, is limited to only one cell type, testis germ cells, where its expression occurs at a particular stage of spermatogenesis, with implications for fertility (*18*, *22*).

Analysis of genomic databases has revealed that the antizymes comprise a family of proteins that is highly conserved among a wide range of eukarya (Figure 1). The antizyme proteins vary from about 150−300 amino acids in length, with most of the sequence variability being associated with the N-terminal residues, while the C-terminal residues are relatively well-conserved. Amino acids 121−227 of AZ-1 (essentially the C-terminal half of the molecule) are sufficient for tight association with ODC, converting ODC into an enzymatically inactive heterodimer. Additional elements needed for stimulating the degradation of ODC by the 26S proteasome are located prior to residue 121 (*23*, *24*), although the first 70 N-terminal residues do not appear to be necessary for simulating ODC degradation.

In addition to ODC, another protein target for antizyme is antizyme inhibitor (AZI). AZI is similar to ODC in that it is also a short-lived protein; however, AZI is degraded at the proteasome in a ubiquitin-dependent manner that does not require interaction with antizyme (*25*). AZI has been shown to release active ODC from antizyme suppression *in vitro* (*26*). AZI shares a significant degree of sequence homology to ODC; however, AZI is enzymatically inactive (*27*). With its ability to sequester antizyme, AZI appears to be another important part of a multicomponent system for

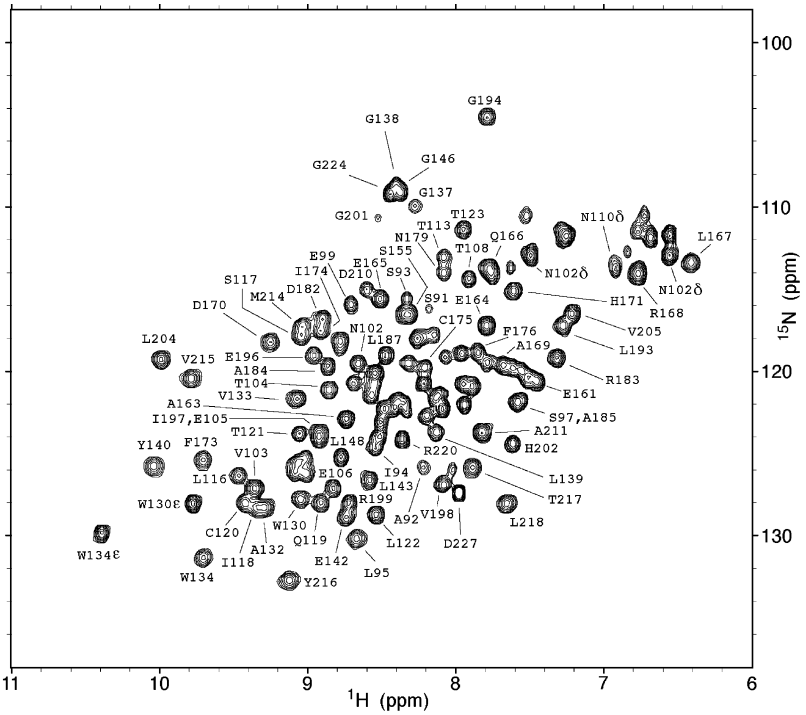

FIGURE 2: Section of the ^{15}N-^{1}H correlated HSQC spectrum of the residues 87−227 of antizyme isoform-1 from rat (AZ-1Δ86) obtained at 22 °C and pH 7. Assignments for the best-resolved cross-peaks are labeled.

regulating polyamines in cells. Antizyme inhibitor regulates all of the isoforms of antizyme (*28*). Recently, Newman et al. (*29*) showed that antizyme binds to the cell-cycle regulatory protein cyclin D1, mediating its degradation by the proteasome without ubiquitination, thus further broadening the range of targets for antizyme.

Despite the biological importance of antizyme, little is known about its structure or the nature of its interactions with its target proteins. The focus of the present work is to describe the structure of a soluble and stable domain of mammalian AZ-1, thus providing an essential framework for furthering understanding antizyme function and how it affects its interaction partners and its role in polyamine regulation.

EXPERIMENTAL PROCEDURES

Protein Cloning, Expression, and Purification. All antizyme coding sequences of *Rattus norvegicus* were derived from cDNA originally provided by Philip Coffino (UCSF). Fragments of antizyme isoform-1 (AZ-1) were expressed in *Escherichia coli* strain HMS174(DE3) with an N-terminal 6×His·Tag using expression plasmid pET30-c(+). The AZ-1 protein lacking the first 69 residues (referred to as AZ-1Δ69) was grown in Luria broth to an OD_{600} of 0.6−1.0, followed by induction of protein expression with 1 mM IPTG. After cell lysis, the AZ-1Δ69 was purified using Ni-NTA affinity chromatography. AZ-1Δ69 was found to have limited solubility, with aggregation at concentrations as low as 1 mg/mL, and was thus unsuitable for study using NMR. A more soluble form of the protein was obtained by removal of the histidine tag and several N-terminal amino acids by limited proteolysis with trypsin. This was accomplished using a 1:100 ratio of trypsin/AZ-1Δ69, with AZ-1Δ69 at a concentration of approximately 0.5 mg/mL, for 30 min at 20 °C followed by the addition of a slight excess of trypsin inhibitor, yielding a protein fragment containing residues 87−227 of AZ-1 (referred to as AZ-1Δ86). The AZ-1Δ86 was further purified by DEAE anion-exchange chromatography and concentrated to approximately 20 mg/mL prior to NMR analysis. The yield of AZ-1Δ86 was typically 50 mg of protein per 6 L of bacterial culture. N-Terminal sequencing and mass spectrometry were used to confirm the identity of the purified AZ-1Δ86 protein. Interestingly, about half of the AZ-1Δ69 expressed in bacterial cells was insoluble, but half of this protein could be refolded by dissolving in 6 M urea, followed by stepwise dialysis into a solution of 0.2 M NaCl and 50 mM phosphate at pH 7. AZ-1Δ86 derived from the refolded protein was identical to that obtained from the protein expressed in soluble form, as judged by NMR spectroscopy. A plasmid encoding the double mutant (R131D and A145D) of AZ-1Δ69 was prepared by QuikChange site-directed mutagenesis (Stratagene), and the mutations were confirmed by DNA sequencing. The double-mutant protein was expressed in *E. coli* and purified using the same methods as for AZ-1Δ86, with a similar yield. Samples of AZ-1Δ86 enriched in ^{15}N and/or ^{13}C were prepared as above but with bacterial growth media containing 0.5 g/L ^{15}N ammonium chloride and/or 2 g/L ^{13}C glucose (Cambridge Isotope Laboratories) as the sources of nitrogen and/or carbon.

NMR Spectroscopy. NMR spectra were recorded at 22 °C using a 500 MHz Varian Inova spectrometer equipped with a triple-resonance cryogenic probe and *z*-axis pulsed field gradient. NMR samples typically contained 1.0−2.0 mM antizyme protein in 90% H_2O/10% D_2O plus 200 mM NaCl and 1 mM sodium azide in a buffer of 50 mM sodium phosphate at pH 7. Backbone resonance assignments (Figure 2) were obtained using three-dimensional HNCA, HNCACB, and HN(CO)CACB spectra (*30*), HNCO spectra (*31*), and HACACBCO spectra (*32*); together these spectra correlate the backbone protons to the N, C^{α}, C, and C^{β} signals of the

same and adjacent amino acid residues. Side-chain resonance assignments were obtained by analyzing three-dimensional ^{15}N-resolved TOCSY−HSQC and ^{13}C-resolved HCCH−TOCSY (*33*) spectra and two-dimensional homonuclear 2QF−COSY and TOCSY spectra. NOE cross-peaks were detected using two-dimensional ^{1}H-^{1}H NOESY, three-dimensional ^{1}H-^{1}H-^{15}N NOESY−HSQC, and three-dimensional ^{1}H-^{1}H-^{13}C NOESY−HSQC (*34*) spectra; the NOE mixing time was 60 ms for spectra used to derive distance constraints. Data were processed using NMR-Pipe (*35*). ^{1}H, ^{15}N, and ^{13}C chemical shifts were referenced as recommended (*36*), with proton chemical shifts relative to internal 2,2-dimethyl-2-silapentane-5-sulfonate (DSS) at 0 ppm. The 0 ppm ^{13}C and ^{15}N reference frequencies were determined by multiplying the 0 ppm ^{1}H reference frequency by 0.251 449 530 and 0.101 329 118, respectively.

Structure Calculation. Structure calculations were performed using the restrained simulated annealing protocol within CNS version 1.1 (*37*), with the goal of identifying the full range of structures that are consistent with the distance and angle restraints derived from the NMR data while having reasonable molecular geometry, consistent with a minimum value of the CNS energy function. Distance restraints were derived from the intensities of cross-peaks within homonuclear 2D NOE and ^{15}N-resolved and ^{13}C-resolved 3D NOE spectra obtained with relatively short mixing times of 60 ms to minimize the effects of spin diffusion. On the basis of the cross-peak intensity in the homonuclear 60 ms NOE spectra, distance restraints were classified as strong (<3.0 Å), medium (<3.6 Å), weak (<4.0 Å), and very weak (<4.5 Å); these distance bounds were calibrated by using interproton distances in regions of regular secondary structure as internal distance standards. Additional cross-peaks observed in the three-dimensional ^{15}N- and ^{13}C-resolved NOE spectra (60 and 80 ms mixing time, respectively) were assigned to distance restraints as strong (<4.0 Å), medium (<5.0 Å), weak (<5.5 Å), and very weak (<6.0 Å). NOE cross-peaks that were only observed in spectra with mixing times of up to 120 ms were assigned a distance restraint of <6.0 Å because of the possibility of spin diffusion. Pseudoatom corrections were applied to the distance restraints as follows: NOEs from valine or leucine methyl groups that were not stereospecifically assigned were measured from the center of the two methyl groups, and 2.5 Å was added to the interproton distance. For NOEs involving other methyl protons, distances were measured from the center of the methyl group and an additional 1.0 Å was added to the interproton distance. For NOEs involving methylene protons with no stereospecific assignment, distances were measured from the center of the methylene group and 0.7 Å was added to the interproton distance. For NOEs involving δ and ϵ protons of tyrosine rings, distances were measured from the center of the two δ protons (or ϵ protons) and 2.4 Å was added to the interproton distance. Backbone dihedral ϕ and ψ angle restraints (to a 60° range) were included for residues that are clearly within regions of regular α-helix and β-strand secondary structure. The α helices and β strands were identified by their characteristic NOE cross-peak patterns, chemical-shift values of the C^{α}, C^{β}, C, and H^{α} nuclei, and patterns of protection of the amide protons from exchange with the solvent upon transfer of the sample to D_2O. Hydrogen bonds were defined using distance bounds for amide protons that were clearly located within regions of regular β-sheet and α-helix structure. Experimental restraints used for the structure calculations and structural statistics are summarized in Table 1.

Table 1: Summary of Refinement and Structural Statistics Obtained for the Rat Antizyme Isoform-1 Protein (AZ-1Δ86)[a]

intraresidue NOEs	497
sequential NOEs (residue *i* to *i* + 1)	426
medium-range NOEs (residue *i* to *i* + 2, 3, 4)	94
long-range NOEs	347
dihederal angle restraints ($\phi + \psi$)	140
hydrogen-bond restraints	56
total structural restraints	1560
rmsd for backbone atoms (residues 94−219) (Å)	2.11
rmsd for side-chain atoms (residues 94−219) (Å)	3.28
rmsd for backbone atoms (residues 94−219, excluding loops 1−4) (Å)	0.89
rmsd for side-chain atoms (residues 94−219, excluding loops 1−4) (Å)	1.83
average number of NOE violations > 0.2 Å (per structure)	11.4
average number of NOE violations > 0.5 Å (per structure)	0
residues in the most favored regions of the Ramachandran plot (%)	73.8
residues in the additional allowed regions of the Ramachandran plot (%)	21.1
residues in generously allowed regions of the Ramachandran plot (%)	4.6
residues in the disallowed regions of the Ramachandran plot (%)	0.5
rmsd for covalent bonds	0.0016
rmsd for covalent angles	0.31
rmsd for improper angles	0.16

[a] Statistics are derived from a set of 24 low-energy structures, each obtained by simulated annealing and derived from a unique starting model; this set is a fair representation of the range of structures that are consistent with the NMR-derived restraints. Intra-side-chain NOE-derived distances with no meaningful structural information were not included in the NOE list.

An initial set of 24 diverse structures was generated from an extended peptide conformation using a simulated annealing protocol with dihedral angle restraints only. Each member of this set was used to generate 10 structures each, via restrained simulated annealing, subject to angle and NMR-derived distance restraints, using different initial trajectories. A set of 24 of refined conformers having the lowest values of the CNS energy function and originating from different starting structures was retained for analysis and evaluation using Procheck-NMR (*38*), with statistics reported in Table 1. These final structures are a fair representation of the full range of structures that are consistent with the experimental data, while having reasonable molecular geometry and having no NOE-derived distance restraint violations greater than 0.5 Å. Searches for similar structures within the Protein Data Bank were carried out using the Vector Alignment Search Tool (VAST), located at the National Center for Biotechnology Information (NCBI) web site, and the DALI search tool (*39*). The coordinates for AZ-1Δ86 have been submitted to the Protein Data Bank and assigned PDB code 1ZO0.

RESULTS

The full-length antizyme isoform-1 (AZ-1) from rats is a 227 amino acid, 26.5-kDa protein. Full-length AZ-1 was found to be insufficiently soluble for NMR studies and did not yield crystals useful for X-ray study despite numerous trials; similar results were obtained for the AZ-1 construct

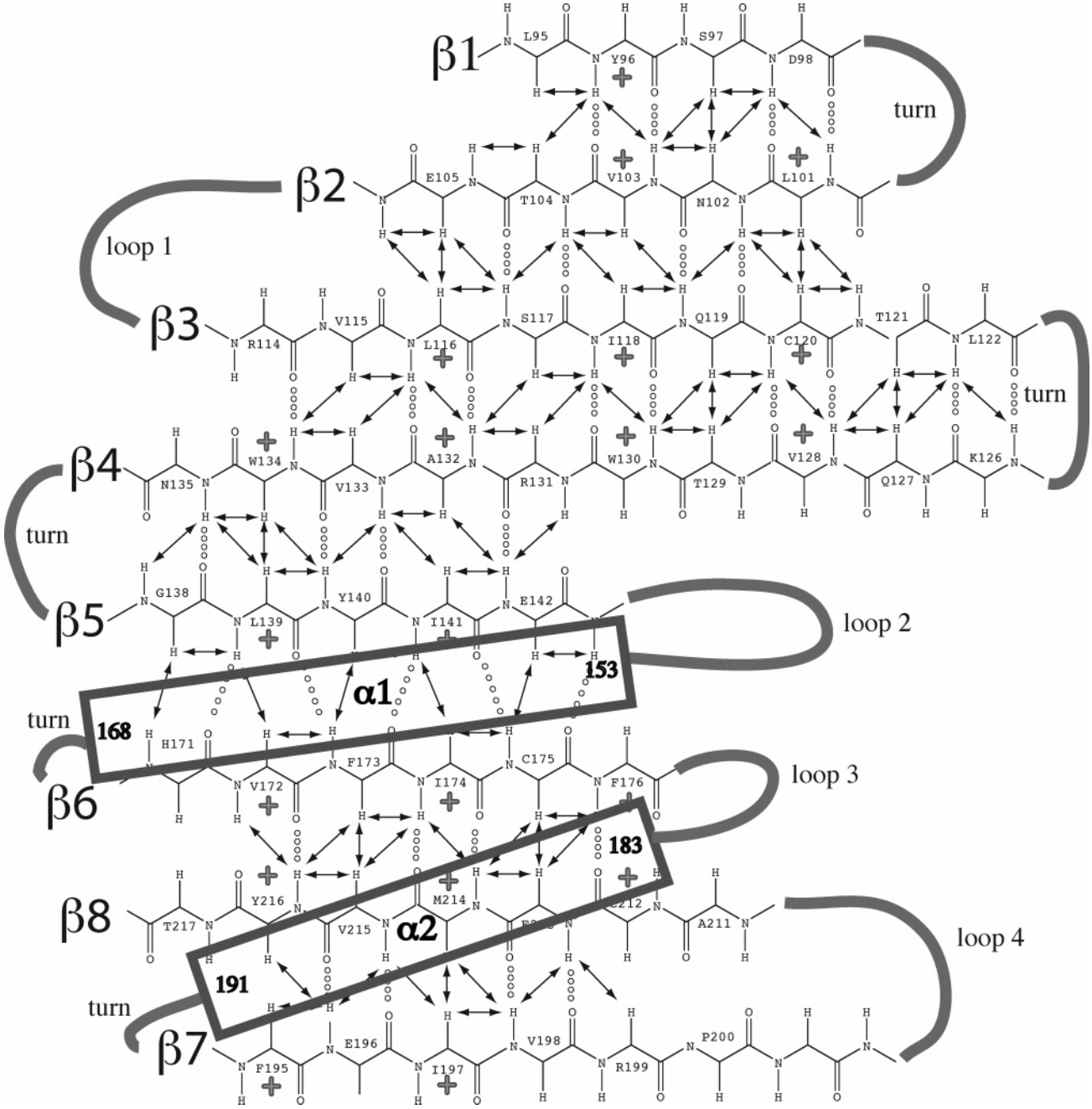

FIGURE 3: Schematic diagram showing the arrangement of elements of secondary structure within AZ-1Δ86, including the eight-stranded β sheet and two α helices. Pairs of protons within the β sheet for which unambiguous NOEs are observed are connected by arrows. Interstrand hydrogen bonds, identified by characteristic NOE cross-peak patterns and relatively slow amide protein exchange times, are indicated by dotted lines. Amino acids labeled with a "+" symbol have side chains that are well-conserved as hydrophobic and are oriented "up" toward the α helices.

lacking the first 69 residues. Interestingly, however, controlled proteolysis experiments using trypsin produced a stable protein fragment consisting of residues 87−227 of the full-length AZ-1. Although this trypsin-resistant fragment (AZ-1Δ86) has not yet yielded crystals, it was found to be sufficiently soluble and stable for characterization by NMR methods. It is noted that forms of AZ-1 that are truncated at the N terminus (AZ-1Δ69 and AZ-1Δ120) have previously been shown to retain ODC binding and inhibition activity (*24*, *40*, *41*), and the N-terminal residues of AZ-1 that are removed by the trypsin treatment are not well-conserved.

The NMR analysis of AZ-1Δ86 was to some extent impeded by a tendency of the protein samples to aggregate over a period of about 24 to 36 h, as indicated by a gradual and substantial broadening of the resonance line widths. It was therefore necessary to prepare a fresh protein sample prior to each multidimensional NMR data collection and restrict data collection times to less than 36 h for each multidimensional spectrum.

Description of the Structure. Results of the NMR analysis show that the dominant structural feature of rat antizyme isoform-1 (AZ-1Δ86) is a single sheet of eight β strands (Figures 3 and 4); the structure also contains two α helices, located on the same side of the β sheet. Within the β sheet, strands $\beta1-\beta5$ are arranged in an antiparallel manner, as are strands $\beta6-\beta8$, while strands $\beta5$ and $\beta6$ are parallel (Figure 3). Compact turns connect secondary structure elements $\beta1-\beta2$, $\beta3-\beta4$, $\beta4-\beta5$, $\alpha1-\beta6$, and $\alpha2-\beta7$; in

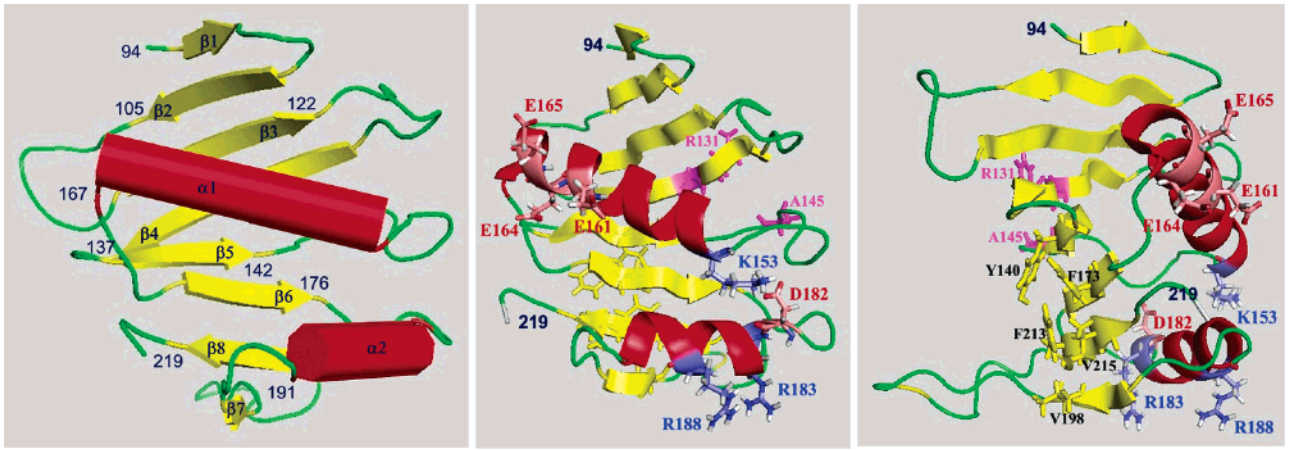

FIGURE 4: Three views of residues 94−219 of the rat antizyme (AZ-1) protein structure. (Left) Schematic diagram of the protein fold, showing the relative positions of the strands and helices. Residue numbers indicate the ends of the secondary structure elements. (Middle) Ribbon diagram of AZ-1, with a view facing the conserved surface residues K153, E161, E164, E165, D182, R183, and R188. Positions of residues R131 and A145 are also shown; mutations of these latter two residues have been shown to change the properties of rat AZ-1 to those of AZ-2 (*21*), as discussed in the text. (Right) Ribbon diagram with a view emphasizing the conserved residues Y140, F173, V198, F213, and F215, which form a hydrophobic patch on the backside of the β sheet opposite the conserved hydrophilic residues. The diagrams were created using PyMol (*54*).

contrast, $\beta2-\beta3$, $\beta5-\alpha1$, $\beta6-\alpha2$, and $\beta7-\beta8$ are connected by relatively extended loops. The eight-stranded β sheet contains a significant twist that allows it to wrap around much of the surface of helix α1 (Figure 4). The protein has a clear and well-defined hydrophobic core, populated by conserved hydrophobic residues indicated in blue in Figure 1. Helix α1 is clearly amphipathic, with Glu161, Glu164, and Glu165 oriented toward the solvent side of the protein. Interestingly, these three residues are conserved as glutamates in nearly all known antizyme sequences (Figure 1) and form a distinct negatively charged patch on the protein surface (Figure 4). The hydrophobic side of helix α1 is oriented toward and packed against the conserved hydrophobic residues of strands $\beta2$, $\beta3$, $\beta4$, and $\beta5$. The shorter of the two helices, α2, is on the same side of the sheet as α1 and has hydrophobic contacts with strands $\beta6$, $\beta7$, and $\beta8$. Well-conserved charged residues of α2 (Asp182, Arg183, and Arg188) are also accessible on the protein surface.

The elements of regular secondary structure (specifically, the two helices and eight strands of the β sheet) are the best-defined regions of the protein structure because of their relatively high density of medium- and long-range NOE-derived distance constraints. Within a family of structures that satisfies the NMR-derived restraints equally well, the root-mean-square deviation (rmsd) is slightly less than 1 Å for the backbone atoms within the helices and β strands, while the loops that connect $\beta2-\beta3$, $\beta5-\alpha1$, $\beta6-\alpha2$, and $\beta7-\beta8$ are less well-defined (Figure 5). Amide protons were not observed for three of the residues of the first of these loops (loop 1), suggesting that it may be disordered or flexible in solution. A relatively low density of medium- and long-range NOE peaks prevented the loop structures from being particularly well-defined by the NMR data. The longest of the loops (loop 4) is the site of insertions of various lengths in antizymes from different species (Figure 1). The least well-defined regions of the structure are the first seven residues at each terminus of the protein; relatively rapid amide proton exchange rates, long T2 relaxation times, and a lack of long-range NOEs indicate that these residues are likely disordered and flexible in solution. AZ-1Δ86 is a monomer in solution,

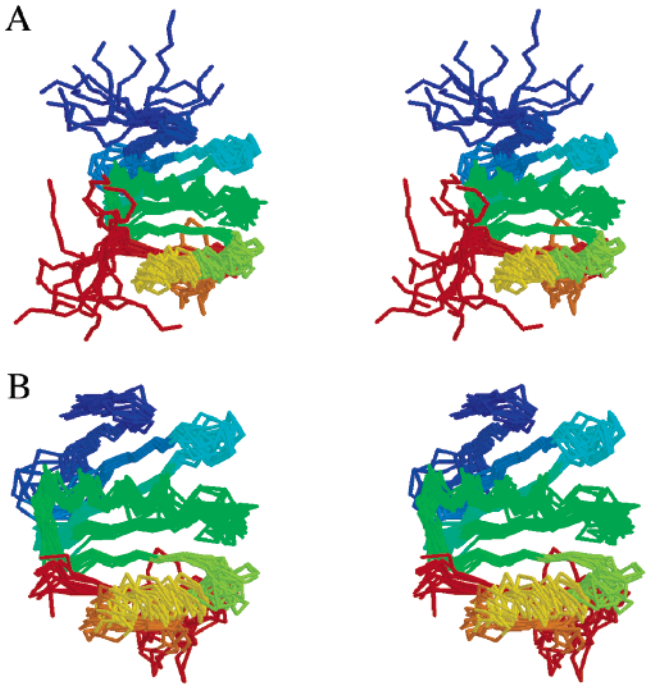

FIGURE 5: Stereoviews showing backbone superpositions for 12 low-energy structures of AZ-1Δ86 that are equally consistent with the NMR data and have the minimum value of the CNS energy function, color-ramped from blue at the N terminus to red at the C terminus. (A) Residues 87−227 of the protein are shown; the figure indicates that the β strands and α helices of the protein are well-defined by the NMR data, while the positions of the first seven and last seven residues are relatively uncertain. (B) Only the backbone atoms of residues 94−219 are used in the superposition. The 12 models are a fair representation of the full range of structures that are consistent with the NMR-derived constraints and reasonable molecular geometry.

indicated by gel-filtration and light-scattering results (data not shown), as well as NMR line widths appropriate for a 16.5-kDa protein domain.

It has been shown that mutating just two residues of rat AZ-1 to those of AZ-2 (Arg131 to Asp and Ala145 to Asp) changes the properties of AZ-1 into those similar to that of AZ-2 (*21*). Specifically, this double mutant of AZ-1 retains

its ability to bind ODC but loses the ability to target ODC for ubiquitin-independent degradation. Although these two residues are not adjacent in the primary sequence of AZ-1, our results show that they are close together in the three-dimensional structure of the protein. Arg131 is located near the center of strand β4, with its positively charged side chain oriented toward the solvent; Ala145 is at the beginning of the loop connecting strand β5 with helix α1 (Figures 3 and 4). A three-dimensional HNCO NMR spectrum of the double mutant of AZ-1Δ86 (Arg131Asp and Ala145Asp) showed that the chemical-shift changes in the backbone resonances are small and localized to the mutated residues and their immediate neighbors. These results indicate that the structural changes introduced by the mutations do not extend significantly beyond the sites of the altered side chains.

DISCUSSION

Antizyme does not appear to have any clear primary sequence similarity to other proteins with known structures. Interestingly, however, an examination of known protein folds within the Structural Classification of Proteins (SCOP) database (*42*) and comparisons with other protein structures carried out using the search tools DALI (*39*) and VAST (available at the NCBI web site) indicate that there are proteins that are clearly similar in fold to that of antizyme, despite the lack of primary sequence similarity and functional relatedness (Figure 6). The most striking structural similarities are between antizyme and members of the Gen5-related (GNAT) family of acetyl transferases (*43*); a representative of this acetyl transferase family is shown in Figure 6. Recent genome-sequencing efforts have identified some 10 000 members of the GNAT family in all kingdoms of life (*43*), and the structures of several of these acetyl transferases have now been solved (*44*, *45*). Representatives of the GNAT acetyl transferases contain the eight strands of antizyme's mixed parallel−antiparallel β sheet, as well as both helices, with all of these elements connected in the same order as in the antizyme (Figure 6); however, the acetyl transferases also contain a mostly helical insertion of typically 50 residues between strands β2 and β3 that antizyme lacks. Interestingly, amino acid sequence similarity indicates that the enzyme spermine-spermidine N^1-acetyltransferase (SSAT) is structurally related to the GNAT transferases, thus establishing a structural link between the polyamine-regulatory protein antizyme and an enzyme that acts on polyamines. SSAT is also similar to antizyme in that its production in cells is induced by polyamines (*46*).

The fold of antizyme is also similar to that of the C-terminal domain of bacterial translation initiation factor IF3 (*47*), with the four β strands and two helices of IF3 corresponding to strands β5−β8 and α1 and α2 of antizyme (Figure 6). Mycothiol synthase (*48*) is another example of a protein with a fold similar to that of antizyme, with the similarity being most apparent when insertions between strands β2 and β3 and strands β7 and β8 are omitted (Figure 6). There is no apparent functional or evolutionary relationship between antizyme and mycothiol synthase; mycothiol is an aminoglycoside synthesized by *Mycobacterium tuberculosis*.

Current models of the antizyme function propose that the monomeric antizyme binds to dimeric ODC, forming inactive heterodimers (*5*, *8*). The affinity of antizyme for ODC is quite high, with the dissociation constant being reported as 10^{-11} M^{-1} (*49*). The structure of the ODC dimer is known from previous crystallographic work (*50*, *51*), where it has been shown that ODC must be homodimeric to be active, because the enzyme active site contains residues from both proteins in the dimer. The binding of antizyme exposes a C-terminal region of ODC; exposure of the ODC C terminus promotes degradation of ODC by the 26S proteasome (*8*). A putative antizyme-binding element (AZBE) has been identified by Coffino (*8*) and located within the ODC structure as part of the surface helices of the TIM barrel that binds the PLP cofactor (*50*, *51*).

Amino acids may be conserved among the various forms of antizyme for reasons related to either structure or function. The majority of the conserved amino acids within antizyme are hydrophobic (indicated in blue in Figure 1) and are

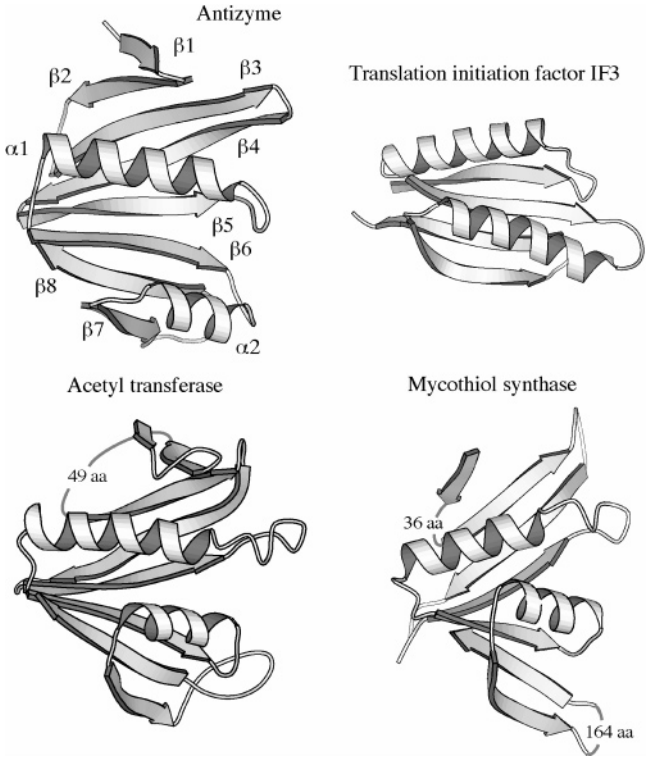

FIGURE 6: Ribbon diagrams comparing antizyme (residues 94−219) with proteins that have some structural similarity, despite their lack of similarity at the level of primary sequence. Strands β5−β8 and helices α1 and α2 of antizyme are similar to the four strands and two helices of the C-terminal domain of translation initiation factor IF3 (PDB entry 1TIG) (*47*); the rmsd between IF3 and the corresponding elements of the antizyme is approximately 3.6 Å. The antizyme is also structurally similar to members of the GNAT family of acetyl transferases; this family includes spermine-spermidine N^1-acetyltransferase (SSAT), an enzyme that acts on polyamines. Shown at the bottom left are residues 3−177 of a representative GNAT acetyl transferase from *Bacillus subtilis* (PDB entry 1NSL) (*45*); a 49-residue mostly helical insertion between strands β2 and β3 has been omitted to clarify the comparison. The rmsd between the backbone of antizyme and the acetyl transferase is approximately 3.5 Å. The antizyme is also similar in structure to a mycothiol synthase from *M. tuberculosis* (PDB entry 1OZP) (*48*). Although the mycothiol synthase does not contain a strand analogous to β1 of antizyme, the other seven strands and two helices are present and connected in the same way in each protein; the similarity is most apparent when two insertions (of 36 and 164 residues) are omitted from the mycothiol synthase structure (lower right). The ribbon diagrams were created using MOLSCRIPT (*55*).

located within the core of the protein; these conserved hydrophobic residues such as Trp130 are likely to be critical for protein folding and stability. The conservation of the hydrophobic core residues provides strong evidence that the known isoforms of antizyme and their homologues in different species are all similar in structure and share the same arrangement of secondary structure elements and fold shown in Figures 3 and 4.

Interestingly, there are a significant number of residues on the protein surface that are strongly conserved among the antizymes (Figure 1). Conserved residues Glu161, Glu164, and Glu165 form a prominent negatively charged patch on the surface of antizyme, on the solvent-side of helix α1, with the acidic side chains oriented away from the β sheet (Figure 4). It has been noted that the AZBE of ODC contains an electropositive surface that might be important for antizyme binding (*50*). It is therefore possible that this negatively charged surface of antizyme may make contact with the AZBE of ODC. Other well-conserved surface residues are Lys153, located at the beginning of helix α1, and Asp182, Arg183, and Arg188, located on the solvent side of helix α2, with side chains oriented away from the sheet (Figure 4). These conserved surface amino acids are candidates for making the essential intermolecular contacts that are common to all of the antizyme homologues and isoforms with their target proteins. Several conserved hydrophobic residues (including Tyr140, Phe173, Val198, Phe213, and Val215) are located within a compact area on the surface of strands β5−β8 that is oriented away from the helices (Figure 4); these residues form an accessible hydrophobic patch that is another potential site for interaction with antizyme partners such as ODC or the proteasome.

The structural results of the present work may also be interpreted in view of previous deletion studies directed toward identifying the minimum functional domain of antizyme. For example, it has been shown that C-terminal residues 219−229 can be deleted from antizyme with little loss of ODC inhibition or binding ability, while additional deletions from the C terminus greatly reduce antizyme activity (*41*). These results are perfectly consistent with the present work, which shows that the ordered domain structure of antizyme ends at residue 219 (Figure 4A). Deletion of antizyme residues 1−144 results in the loss of ability to bind and inhibit ODC, while residues 1−112 can be deleted with reduced (but not completely abolished) ODC-binding activity or destabilization (*41*); this latter result suggests that strands β1−β2 may not be essential for antizyme function. Similarly, a previous study has shown that the ability of antizyme to regulate polyamine transport resides in residues 119−216 (*52*), suggesting that strands β1−β3 may not be absolutely essential in forming the active antizyme; these three β strands do not contain any of the residues that we have identified as being most likely to be involved in intermolecular interactions (Figure 4). Antizyme residues 106−212 have been reported as being sufficient for binding ODC; however, residues prior to 106 are needed for stimulating ODC degradation (*24*).

In summary, the structural model for antizyme provides an essential framework for a further understanding of how this unusual and biologically important protein affects its interaction partners and its role in polyamine regulation. Although the details of the antizyme−ODC binding interaction cannot be fully understood in the absence of a structure for the heterodimeric complex, the present work does provide significant information that will be useful in designing additional experiments to identify which surfaces of antizyme are involved in making specific intermolecular contacts.

REFERENCES

1. Heller, J. S., Fong, W. F., and Canellakis, E. S. (1976) Induction of a protein inhibitor to ornithine decarboxylase by the end products of its reaction, *Proc. Natl. Acad. Sci. U.S.A. 73*, 1858−1862.
2. Childs, A. C., Mehta, D. J., and Gerner, E. W. (2003) Polyamine-dependent gene expression, *Cell. Mol. Life Sci. 60*, 1394−1406.
3. Wallace, H., Fraser, A., and Hughes, A. (2003) A perspective of polyamine metabolism, *Biochem. J. 376*, 1−14.
4. Coffino, P. (2001) Regulation of cellular polyamines by antizyme, *Nat. Rev. Mol. Cell. Biol. 2*, 188−194.
5. Coffino, P. (2001) Antizyme, a mediator of ubiquitin-independent proteasomal degradation, *Biochimie 83*, 319−323.
6. Murakami, Y., Matsufuji, S., Kameji, T., Hayashi, S., Igarashi, K., Tamura, T., Tanaka, K., and Ichihara, A. (1992) Ornithine decarboxylase is degradaded by the 26S proteasome without ubiquitination, *Nature 360*, 597−600.
7. Hayashi, S., Murakami, Y., and Matsufuji, S. (1996) Ornithine decarboxylase antizyme: A novel type of regulatory protein, *Trends Biochem. Sci. 21*, 27−30.
8. Coffino, P. (1998) Degradation of ornithine decarboxylase, in *Ubiquitin and the Biology of the Cell* (Peters, J. M., Harris, J. R., and Finley, D., Eds.) pp 411−427, Plenum Press, New York.
9. Zhang, M., Pickart, C. M., and Coffino, P. (2003) Determinants of proteasome recognition of ornithine decarboxylase, a ubiquitin-independent substrate, *EMBO J. 22*, 1488−1496.
10. Zhang, M., MacDonald, A., Hoyt, M. A., and Coffino, P. (2004) Proteasomes begin ornithine decarboxylase digestion at the C-terminus, *J. Biol. Chem. 279*, 20959−20965.
11. Chen, X., Chi, Y., Bloecher, A., Aebersold, R., Clurman, B., and Roberts, J. (2004) *N*-Acetylation and ubiquitin-independent proteasomal degradation of $p21^{Cip1}$, *Mol. Cell 16*, 839−847.
12. Matsufuji, S., Matsufuji, T., Miyazaki, Y., Murakami, Y., Atkins, J. F., Gesteland, R. F., and Hayashi, S. I. (1995) Autoregulatory frameshifting in decoding mammalian ornithine decarboxylase antizyme, *Cell 80*, 51−60.
13. Rom, E., and Kahana, C. (1994) Polyamines regulate the expression of ornithine decarboxylase antizyme *in vitro* by inducing ribosomal frame-shifting, *Proc. Natl. Acad. Sci. U.S.A. 91*, 3959−3963.
14. Ivanov, I. P., Matsufuji, S., Murakami, Y., Gesteland, R. F., and Atkins, J. F. (2000) Conservation of polyamine regulation by translational frameshifting from yeast to mammals, *EMBO J. 19*, 1907−1917.
15. Kankare, K., Uusi-Oukari, M., and Janne, O. A. (1997) Structure, organization, and expression of ornithine decarboxylase antizyme gene, *Biol. J. 324*, 807−813.
16. Ivanov, I. P., Gesteland, R. F., and Atkins, J. F. (1998) A second mammalian antizyme: Conservation of programmed ribosomal frameshifting, *Genomics 52*, 119−129.
17. Ivanov, I. P., Anderson, C. B., Gesteland, R. F., and Atkins, J. F. (2004) Identification of a new antizyme mRNA +1 frameshifting stimulatory pseudoknot in a subset of diverse invertebrates and its apparent absence in intermediate species, *J. Mol. Biol. 339*, 495−504.
18. Ivanov, I. P., Rohrwasser, A., Terreros, D. A., Gesteland, R. F., and Atkins, J. F. (2000) Discovery of a spermatogenesis stage-specific ornithine decarboxylase antizyme: Antizyme 3, *Proc. Natl. Acad. Sci. U.S.A. 97*, 4808−4813.
19. Mitchell J. L., Judd, G. G., Bareyal-Leyser, A., and Ling, S. Y. (1994) Feedback repression of polyamine transport is mediated by antizyme in mammalian tissue-culture cells, *Biochem. J. 299*, 19−22.
20. Zhu, C., Lang, D. W., and Coffino, P. (1999) Antizyme-2 is a negative regulator of ornithine decarboxylase and polyamine transport, *J. Biol. Chem. 274*, 26425−26430.
21. Chen, H., MacDonald, A., and Coffino, P. (2002) Structural elements of antizymes 1 and 2 are required for proteasomal degradation of ornithine decarboxylases, *J. Biol. Chem. 277*, 45957−45961.

22. Tosaka, Y., Tanaka, H., Yano, Y., Masai, K., Nozaki, M., Yomogida, K., Otani, S., Nojima, H., and Nishimune, Y. (2000) Identication and characterization of testis specific ornithine decarboxylase antizyme (OAZ-t) gene: Expression in haploid germ cells and polyamine-induced frameshifting, *Genes Cells 5*, 265−276.
23. Li, X., and Coffino, P. (1993) Degradation of ornithine decarboxylase: Exposure of the C-terminal target by a polyamine-inducible inhibitory protein, *Mol. Cell. Biol. 13*, 2377−2383.
24. Li, X., and Coffino, P. (1994) Distinct domains of antizyme required for binding and proteolysis of ornithine decarboxylase, *Mol. Cell. Biol. 14*, 87−92.
25. Bercovich, Z., and Kahana, C. (2004) Degradation of antizyme inhibitor, an ornithine decarboxylase homologous protein, is ubiquitin-dependent and is inhibited by antizyme, *J. Biol. Chem. 279*, 54097−54102.
26. Nilsson, J., Grahn, B., and Heby, O. (2000) Antizyme inhibitor is rapidly induced in growth-stimulated mouse fiberblasts and releases ornithine decarboxylase from antizyme suppression, *Biochem. J. 346*, 699−704.
27. Murakami, Y., Ichiba, T., Matsufuji, S., and Hayashi, S. (1996) Antizyme inhibitor, a highly homologous protein to ornithine decarboxylase, *J. Biol. Chem. 271*, 3340−3342.
28. Mangold, U., and Leberer, E. (2005) Regulation of all members of the antizyme family by antizyme inhibitor, *Biochem. J. 385*, 21−28.
29. Newman, R., Mobascher, A., Mangold, U., Koike, C., Diah, S., Schmidt, M., Finley, D., and Zetter, B. (2004) Antizyme targets cyclin D1 for degradation: A novel mechanism for cell growth repression, *J. Biol. Chem. 279*, 41504−41511.
30. Muhandiram, D. R., and Kay, L. E. (1994) Gradient-enhanced triple resonance three-dimensional NMR experiments with improved sensitivity, *J. Magn. Reson. B 103*, 203-216.
31. Grzesiek, S., and Bax, A. (1992) ^{1}H, ^{13}C, and ^{15}N NMR backbone assignments and secondary structure of human interferon-γ, *J. Magn. Reson. 96*, 432−440.
32. Kay, L. E. (1993) Pulsed-field gradient-enhanced three-dimensional NMR experiment for correlating ^{13}Cα, ^{13}C′, and ′Hα chemical shifts in uniformly ^{13}C-labeled proteins dissolved in H_2O, *J. Am. Chem. Soc. 115*, 2055−2057.
33. Kay, L. E., Xu, G. Y., Singer, A. U., Muhandiram, D. R., and Forman-Kay, J. D. (1993) A gradient-enhanced HCCH-TOCSY experiment for recording side-chain ^{1}H and ^{13}C correlations in H_2O samples of proteins, *J. Magn. Reson. B 101*, 333−337.
34. Pascal, S. M., Muhandiram, D. R., Yamazaki, T., Forman-Kay, J. D., and Kay, L. E. (1994) Simultaneous acquisition of ^{15}N- and ^{13}C-edited NOE spectra of proteins dissolved in H_2O, *J. Magn. Reson. B 103*, 197−201.
35. Delaglio, F., Grzesiek, S., Vuister, G. W., Zhu, G., Pfeifer, J., and Bax, A. (1995) NMRPipe: A multidimensional spectral processing system based on UNIX pipes, *J. Biomol. NMR 6*, 277−293.
36. Wishart, D. S., Bigam, C. G., Yao, J., Abildgaard, F., Dyson, H. J., Oldfield, E., Markley, J. L., and Sykes, B. D. (1995) ^{1}H, ^{13}C, and ^{15}N chemical shift referencing in biomolecular NMR, *J. Biomol. NMR 6*, 135−140.
37. Brünger, A. T., Adams, P. D., Clore, G. M., DeLano, W. L., Gros, P., Grosse-Kunstleve, R. W., Jiang, J. S., Kuszewski, J., Nilges, M., Pannu, N. S., Read, R. J., Rice, L. M., Simonson, T., and Warren, G. L. (1998) Crystallography and NMR system: A new software suite for macromolecular structure determination, *Acta Crystallogr., Sect. D: Biol. Crystallogr. 54* (part 5), 905−921.
38. Laskowski, R. A., Rullmann, J. A., MacArthur, M. W., Kaptein, R., and Thornton, J. M. (1996) AQUA and PROCHECK-NMR: Programs for checking the quality of protein structures solved by NMR, *J. Biomol. NMR 8*, 477−486.
39. Holm, L., and Sander, C. (1993) Protein structure comparison by alignment of distance matrices, *J. Mol. Biol. 233*, 123−138.
40. Li, X., and Coffino, P. (1992) Regulated degradation of ornithine decarboxylase requires interaction with the polyamine-inducible protein antizyme, *Mol. Cell. Biol. 12*, 3556−3562.
41. Ichiba, T., Matsufuji, S., Miyazaki, Y., Murakami, Y., Tanaka, K., Ichihara, A., and Hayashi, S. (1994) Functional regions of ornithine decarboxylase antizyme, *Biochem. Biophys. Res. Commun. 200*, 1721−1727.
42. Murzin, A. G., Brenner, S. E., Hubbard, T., and Chothia, C. (1995) SCOP: A structural classification of proteins database for the investigation of sequences and structures, *J. Mol. Biol. 247*, 536−540.
43. Vetting, M. W., de Carvalho, L. P., Yu, M., Hegde, S. S., Magnet, S., Roderick, S. L., and Blanchard, J. S. (2005) Structure and functions of the GNAT superfamily of acetyltransferases, *Arch. Biochem. Biophys. 433*, 212−226.
44. Poux, A. N., Cebrat, M., Kim, C. M., Cole, P. A., and Marmorstein, R. (2002) Structure of the GCN5 histone acetyltransferase bound to a bisubstrate inhibitor, *Proc. Natl. Acad. Sci. U.S.A. 99*, 14065−14070.
45. Brunzelle, J. S., Wu, R., Korolev, S. V., Collart, F. R., Joachimiak, A., and Anderson, W. F. (2004) Crystal structure of *Bacillus subtilis* YdaF protein: A putative ribosomal *N*-acetyltransferase, *Proteins 57*, 850−853.
46. Coleman, C. S., and Pegg, A. E. (2001) Polyamine analogues inhibit the ubiquitination of spermine/spermidine N^1-acetyltransferase and prevent its targeting to the proteasome for degradation, *Biochem. J. 358*, 137−145.
47. Biou, V., Shu, F., and Ramakrishnan, V. (1995) X-ray crystallography shows that translational initiation factor IF3 consists of two compact α/β domains linked by an α-helix, *EMBO J. 14*, 4056−4064.
48. Vetting, M. W., Roderick, S. L., Yu, M., and Blanchard, J. S. (2003) Crystal structure of mycothiol synthase (Rv0819) from *Mycobacterium tuberculosis* shows structural homology to the GNAT family of *N*-acetyltransferases, *Protein Sci. 12*, 1954−1959.
49. Kitani, T., and Fujisawa, H. (1984) Purification and some properties of a protein inhibitor (antizyme) of ornithine decarboxylase from rat liver, *J. Biol. Chem. 259*, 10036−10040.
50. Kern, A. D., Oliveira, M. A., Coffino, P., and Hackert, M. L. (1999) The structure of mammalian ornithine decarboxylase at 1.6 Å resolution: Stereochemical implications of PLP-dependent amino acid decarboxylases, *Structure 7*, 567−581.
51. Almrud, J. J., Oliveira, M. A., Kern, A. D., Grishin, N. V., Phillips, M. A., and Hackert, M. L. (2000) Crystal structure of human ornithine decarboxylase at 2.1 Å resolution: Structural insights to antizyme binding, *J. Mol. Biol. 295*, 7−16.
52. Sakata, K., Fukuchi-Shimogori, T., Kashiwagi, K., and Igarashi, K. (1997) Identification of regulatory region of antizyme necessary for the negative regulation of polyamine transport, *Biochem. Biophys. Res. Commun. 238*, 415−419.
53. Palanimurugan, R., Scheel, H., Hofmann, K., and Dohmen, R. (2004) Polyamines regulate their synthesis by inducing expression and blocking degradation of ODC antizyme, *EMBO J. 23*, 4857−4867.
54. DeLano, W. L. (2002) The PyMol Molecular Graphics System, DeLano Scientific, San Carlos, CA.
55. Kraulis, P. J. (1991) MOLSCRIPT: A program to produce both detailed and schematic plots of protein structures, *J. Appl. Crystallogr. 24*, 946−950.

BI051081K